## Nonreciprocal single-photon band structure

Jiangshan Tang, <sup>1,2</sup> Wei Nie, <sup>3</sup> Lei Tang, <sup>1</sup> Mingyuan Chen, <sup>1</sup> Xin Su, <sup>1,4</sup> Yanqing Lu, <sup>1,2</sup> Franco Nori, <sup>3,5</sup> and Keyu Xia<sup>1,2,6,\*</sup>

College of Engineering and Applied Sciences, National Laboratory of Solid State Microstructures, and Collaborative Innovation Center of Advanced Microstructures, Nanjing University, Nanjing 210023, China
 School of Physics, Nanjing University, Nanjing 210023, China
 RIKEN Quantum Computing Center, RIKEN Cluster for Pioneering Research, Wako-shi, Saitama 351-0198, Japan
 School of Electronic Science and Engineering, Nanjing University, Nanjing 210023, China
 Physics Department, The University of Michigan, Ann Arbor, Michigan 48109-1040, USA
 Jiangsu Key Laboratory of Artificial Functional Materials, Nanjing University, Nanjing 210023, China
 (Dated: November 12, 2021)

We study single-photon band structure in a one-dimensional (1D) coupled-resonator optical waveguide (CROW) which chirally couples to an array of two-level quantum emitters (QEs). The chiral interaction between the resonator mode and the QE can break the time-reversal symmetry without the magneto-optical effect. As a result, a nonreciprocal single-photon edge state, band gap and flat band appear. By using such a chiral QE-CROW system, including a finite number of unit cells and working in the nonreciprocal band gap, we achieve frequency-multiplex single-photon circulators with high fidelity and low insertion loss. The chiral QE-light interaction can also protect one-way propagation of single photons against backscattering. Our work opens a new door for studying nonreciprocal photonic band structure and exploring its applications in the quantum regime.

Introduction.—Optical nonreciprocity plays an indispensable role in many important applications including quantum-information processing [1], invisible sensing [2, 3], noise-free information processing [4] and unconventional lasing [5, 6]. Conventional nonreciprocal optical devices breaking the time-reversal symmetry rely on the weak magneto-optical effect and are difficult to be integrated on a chip due to the constraint of a strong magnetic field.

Various theoretical schemes and experimental methods have been reported to circumvent the constraint of magnetic fields by using optical nonlinearity [7–14], optomechanical resonators [15–17], spinning resonators [18, 19], tempospatial modulation of the medium [20–22] or chiral quantum optics systems [23–31]. In contrast to classical methods, a chiral quantum optics system can realize optical nonreciprocity in the quantum regime [9–11, 24–26, 28] and can perform chiral quantum information processing [32–35].

It is of great interest to study photon behavior under the chiral interaction between quantum emitters (QEs) and a coupled resonator array. The chiral interaction of some OEs with few resonators has been extensively studied and promises many important applications [36, 37]. Although the coupledresonator optical waveguide (CROW) has been widely investigated [38-42], the optical chirality in the CROW is barely addressed. In analogy to the electronic band structure in condensed matter, a periodic photonic structure exhibits nontrivial band structures and allows defect-immune photon transport [43–47]. Nevertheless, such topological optical system can break time-reversal symmetry and is appealing for backscattering-immune optical isolation only in the presence of an external/synthetic magnetic field. Thus, it is highly desirable to achieve one-way photonic band structure such as nonreciprocal single-photon edge states (SPESs) and band gap without magnetic fields, in particular, in the quantum regime.

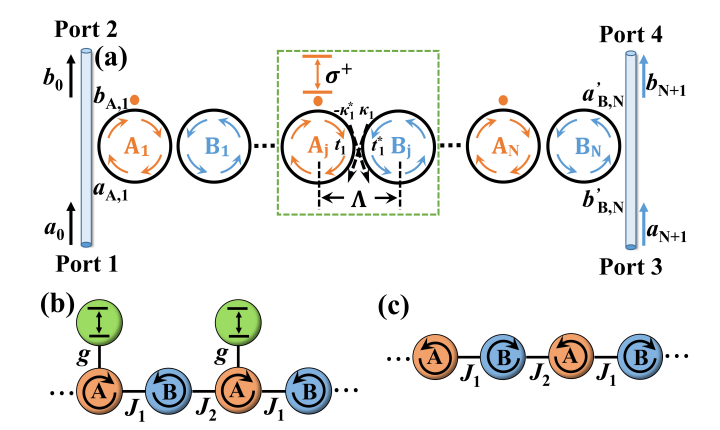


FIG. 1. (a) Schematic of a chiral QE-CROW system containing N unit cells and the input and output waveguides. The arrows represent the circulating direction of the whispering-gallery mode for an input to port 1 or 3 (forward input). The photon incident to ports 2 and 4 (backward input) excites the oppositely propagating resonator modes. The QEs with  $\sigma^+$ -polarized optical transition are periodically coupled to the clockwise resonator mode of the sublattice A in each unit cell, see dashed box. (b) The L-type trimer chain in the forward-input case. (c) The dimer chain for the backward-input case.

By exploring the chiral interaction between an array of QEs and a 1D CROW, here we show that nonreciprocal single-photon band structure, including SPES, band gap and flat band, can be achieved without a magnetic field. Interestingly, we can conduct frequency-multiplex single-photon circulators with such a chiral QE-CROW system working in the nonreciprocal band gap. Our circulator is immune to backscattering.

System and model.—The schematic of the chiral QE-CROW system is depicted in Fig. 1. In the CROW, the evanescent field of each microring resonator is almost perfectly circularly polarized and thus possesses nearly unitary optical chirality [24, 25, 31], i.e. possessing spin-momentum locking [48–51]. In each unit cell, the adjacent resonators are sepa-

<sup>\*</sup> keyu.xia@nju.edu.cn

rated by  $\Lambda$  and coherently coupled via evanescent fields. Each resonator supports two degenerate optical whispering-gallery modes circulating along either the clockwise (CW) or counterclockwise (CCW) direction. We divide the resonators into A and B sublattice groups, respectively denoted as R<sub>A</sub> and  $R_B$ . In each unit cell, a two-level QE with frequency  $\omega_q$  is only embedded in the A-sublattice resonator RA, but decouples from the B-sublattice resonator R<sub>B</sub>. Within a cell, the CW (CCW) mode of R<sub>A</sub> couples to the CCW (CW) mode of  $R_B$  with strength  $J_1$ , see the green box in Fig. 1(a). The jth resonator  $R_A$  couples to the (j + 1)th resonator  $R_B$  in the next cell with strength  $J_2$ . The oppositely circulating whisperinggallery modes in the sublattices A and B form N unit cells with a lattice constant of  $2\Lambda$  [39, 52]. We assume that the resonators, with resonance frequency  $\Omega$  and internal dissipation rate  $\gamma_{in}$ , are identical.

Hereafter, we consider only a single excitation in the QE-CROW system. The QEs can be precisely positioned atoms [25, 40, 53], quantum dots [37, 54, 55], or nanopillars covered by monolayers [56, 57]. By optically initializing the QEs in specific spin ground states or shifting the transition energy with a circularly-polarized field via the optical Stark effect, we can induce a chiral transition in the QE. Without loss of generality, we assume that the QE transition and the evanescent field of the CW mode of  $R_A$  are both  $\sigma_+$ -polarized. In this arrangement, we create a chiral interaction between the QE and the CW mode of  $R_A$  without using a magnetic field [23–26, 29–31]. However, the QE decouples from the CCW mode [24–26, 31].

When a single photon is incident into port 1 or 3, namely the forward-input case, the CW modes in the  $R_A$  resonators and the CCW ones in the  $R_B$  resonators are driven. We refer to this excitation as the  $CW_A$  –  $CCW_B$  supermode (opposite to the  $CCW_A$  –  $CW_B$  supermode). In this case, the QEs are coupled to  $R_A$  in each unit cell. The QE-CROW system is equivalent to an L-type trimer chain with each cell containing three sublattices, see Fig. 1(b). We take  $\omega_q = \Omega$  and can write the Hamiltonian of the system in the rotating frame as:

$$\hat{H}_{\text{CW}_{A}-\text{CCW}_{B}} = \sum_{j}^{N} \left( g \hat{a}_{j,\cup}^{\dagger} \hat{\sigma}_{j} + J_{1} \hat{a}_{j,\cup}^{\dagger} \hat{b}_{j,\cup} + \text{H.c.} \right) + \sum_{j}^{N-1} \left( J_{2} \hat{a}_{j+1,\cup}^{\dagger} \hat{b}_{j,\cup} + \text{H.c.} \right),$$

$$(1)$$

where  $\hat{a}_{j,\cup}$  ( $\hat{b}_{j,\cup}$ ) is the annihilation operator of the CW (CCW) mode of the  $R_A$  ( $R_B$ ) resonator in the *j*th unit cell, and  $\hat{\sigma}_j$  denotes the lowering operator of the *j*th two-level QE.

Now we study the band structure of an infinite 1D-CROW model in a single-excitation subspace. We assume a periodic boundary condition along the 1D-CROW chain and apply the Fourier transform,  $\zeta_j = \left(1/\sqrt{N}\sum_k e^{ikj}\zeta_k\right)$  with  $\zeta_j = \left(\hat{a}_{j,\cup},\hat{\sigma}_j,\hat{b}_{j,\cup}\right)^T$ , to Eq. (1), thus,  $\hat{H}_{\text{CW}_A-\text{CCW}_B} = \sum_k \zeta_{\iota}^{\dagger} \hat{H}_{\text{CW}_A-\text{CCW}_B}(k)\zeta_k$ . Then, the Hamiltonian takes the following

lowing form in wavevector space

$$\hat{H}_{\text{CW}_A-\text{CCW}_B}(k) = \begin{pmatrix} 0 & g & J_1 + J_2 e^{-ik} \\ g & 0 & 0 \\ J_1 + J_2 e^{ik} & 0 & 0 \end{pmatrix}.$$
 (2)

In comparison, if a single photon incidents to port 2 or 4 corresponding to the backward-input case, then the  $CCW_A - CW_B$  supermode is driven in each unit cell and the QEs decouple from all resonators. Our system reduces to a dimer chain, corresponding to a standard Su-Schrieffer-Heeger (SSH) model [58, 59], see Fig. 1(c). The Hamiltonian then becomes

$$\hat{H}_{\text{CCW}_A-\text{CW}_B}(k) = \begin{pmatrix} 0 & J_1 + J_2 e^{-ik} \\ J_1 + J_2 e^{ik} & 0 \end{pmatrix}.$$
 (3)

The band structures and energy spectra of the system in the  $CW_A - CCW_B$  and  $CCW_A - CW_B$  supermodes can be found by solving the eigenvalues and eigenstates of Eq. (2) and Eq. (3), respectively. In the case related to the  $CW_A - CCW_B$  supermode, the QEs interact with the RA resonators. This interaction causes a phase and amplitude modulation  $e^{i\varphi}$  to the R<sub>A</sub> CW mode [60, 61]. Here,  $\varphi$  is a complex number. In contrast, the QE-resonator interaction is absent for the  $CCW_A - CW_B$ supermode. Thus, the extra modulation disappears, i.e.  $\varphi = 0$ . The dispersion relations of the  $CW_A - CCW_B$  supermode consists of three dispersive bands. It is essentially different from the  $CCW_A - CW_B$  supermode, which only contains two bands. Therefore, the single-photon band structures are nonreciprocal in two counter-propagating cases. This nonreciprocal single-photon dispersion occurs because the chiral QE-light coupling breaks the time-reversal symmetry of the system.

A finite 1D-CROW chain with a large number of unit cells can approximately exhibit the property of an infinite chain [39]. Next, we discuss a finite chiral 1D CROW containing N unit cells ( $N \ge 1$ ) and evaluate the single-photon transmission. Two optical waveguides are side-coupled to the terminal resonators as input and output channels. We utilize the transfer matrix method to investigate the transmission properties of the system [41, 60]. We consider the forward case. The notations for the field components  $\{a\}$  and  $\{b\}$  are shown in Fig. 1(a). By successively multiplying the transfer matrices of all the coupling relations, we obtain the transport relation

$$\begin{pmatrix} a_{N+1} \\ b_{N+1} \end{pmatrix} = M \begin{pmatrix} a_0 \\ b_0 \end{pmatrix} \equiv \begin{pmatrix} M_{11} & M_{12} \\ M_{21} & M_{22} \end{pmatrix} \begin{pmatrix} a_0 \\ b_0 \end{pmatrix} , \qquad (4)$$

 $M = M_{\text{out}} M_{\text{p,B}} M_{\text{c,1}} M_{\text{p,A}} (M_{\text{c,2}} M_{\text{p,B}} M_{\text{c,1}} M_{\text{p,A}})^{N-1} M_{\text{in}}$ , where

$$\begin{split} M_{\rm p,A} &= \begin{pmatrix} \alpha e^{-i\theta} & 0 \\ 0 & \alpha e^{i(\theta+\varphi)} \end{pmatrix}, \quad M_{\rm p,B} &= \begin{pmatrix} \alpha e^{-i\theta} & 0 \\ 0 & \alpha e^{i\theta} \end{pmatrix}, \\ M_{\rm c,1} &= \frac{1}{\kappa_1} \begin{pmatrix} 1 & -t_1 \\ t_1^* & -1 \end{pmatrix}, \quad M_{\rm c,2} &= \frac{1}{\kappa_2} \begin{pmatrix} 1 & -t_2 \\ t_2^* & -1 \end{pmatrix}, \\ M_{\rm in} &= \frac{1}{\kappa_{\rm in}} \begin{pmatrix} -t_{\rm in} & 1 \\ -1 & t_{\rm in}^* \end{pmatrix}, \quad M_{\rm out} &= \frac{1}{\kappa_{\rm out}} \begin{pmatrix} 1 & -t_{\rm out} \\ t_{\rm out}^* & -1 \end{pmatrix}. \end{split}$$
 (5)

We define  $\{t_{\text{in}}, t_1, t_2, t_{\text{out}}\}$  and  $\{\kappa_{\text{in}}, \kappa_1, \kappa_2, \kappa_{\text{out}}\}$  as the transmission and coupling coefficients of the intrasite and intersite resonators, where  $t_i$  (i = in, 1, 2, out) is a real number,  $\kappa_i$  is an

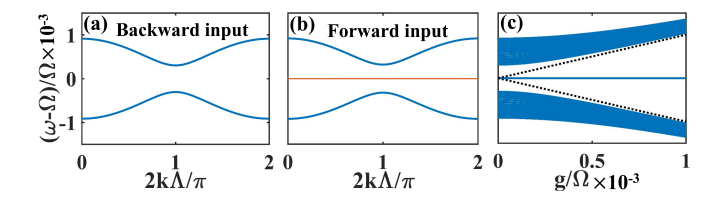


FIG. 2. Single-photon band structures of the chiral QE-CROW system in the case of  $J_1 < J_2$ . (a) Band structure when the  $CCW_A - CW_B$  supermode is excited in the absence of the QEs, i.e.,  $g/\Omega = 0$ . (b) Band structure when the  $CW_A - CCW_B$  supermode, coupling to the QEs with  $g/\Omega = 10^{-4}$ , is driven. (c) Band structure versus the coupling strength g when the  $CW_A - CCW_B$  supermode is driven. Other parameters are  $J_1/\Omega = 3 \times 10^{-4}$ ,  $J_2 = 2J_1$ .

imaginary number, and  $|t_i|^2 + |\kappa_i|^2 = 1$  [41]. Above,  $\theta$  indicates the phase change and  $\alpha$  is the loss coefficient of propagating single photons. This can be calculated as  $\alpha \approx 1 - 2\gamma_{\rm in}/\mathcal{F}$  from the intrinsic loss rate  $\gamma_{\rm in}$  of the resonator [61], where  $\mathcal{F}$  is the free spectral range of the resonator considered here. The ratio  $\kappa_{\rm in}/\mathcal{F}$  is negligible for our high-quality resonators. Thus, hereafter we can take  $\alpha \approx 1$ .

For simplicity, we assume  $\kappa_{\rm in} = \kappa_{\rm out}$  ( $t_{\rm in} = t_{\rm out}$ ). The external losses of the edge resonators  $A_1$  and  $B_{\rm N}$  are  $\gamma_{\rm ex} = \gamma_{\rm ex,1} = \gamma_{\rm ex,N} = -\ln{(|t_{\rm in}|)} \times \mathcal{F}$ . Considering a single-photon entering port 1 ( $a_{\rm N+1} = 0$ ), we obtain the transmission matrix elements between the input and output ports:

$$T_{12} = \left| \frac{b_0}{a_0} \right|^2 = \left| \frac{M_{11}}{M_{12}} \right|^2 ,$$
 (6a)

$$T_{14} = \left| \frac{b_{N+1}}{a_0} \right|^2 = \left| M_{21} - \frac{M_{11} M_{22}}{M_{12}} \right|^2 ,$$
 (6b)

where  $T_{mn}$  is the transmission from port m to port n, with m, n = 1, 2, 3, 4. Because the input to port 3 excites the  $CW_A - CCW_B$  supermode circulating along the same direction, we have  $T_{12} = T_{34}$  and  $T_{14} = T_{32}$ . When the  $CCW_A - CW_B$  supermode is excited in the backward case, the QEs decouple from the resonators and we have  $\varphi = 0$ . Therefore, we have  $T_{mn} \neq T_{nm}$  for  $m \neq n$ , indicating the occurrence of optical nonreciprocity in our chiral QE-CROW system.

Below, we consider an ideal scenario in which the QE dissipation rate  $\gamma$  is negligible compared to the coupling strength g. For simplicity, we set  $\gamma = 0$ .

Nonreciprocal single-photon flat band and edge states.— We first discuss the case  $J_1 < J_2$ . As seen from the dispersion relations in Fig. 2, the QE-CROW system exhibits a nonreciprocal single-photon band structure. Typically, two dispersive bands of the SSH model appear in the backward case, as shown in Fig. 2(a) [62] for  $J_1/\Omega = 3 \times 10^{-4}$  and  $J_2 = 2J_1$ . The curves with opposite slopes imply two opposite directions of single-photon propagation, corresponding to the input to port 2 or 4 in Fig. 1, respectively. In the forward case, the QEs interact with the  $R_A$  resonator. A flat band appears at  $\omega = \Omega$  due to the coupling to the QEs, dividing the original band gap into two parts, see Fig. 2(b). Thus, our QE-CROW system allows slow light and delay of single-photon pulses [63–65]. As the QE-resonator coupling strength increases, the two band gaps

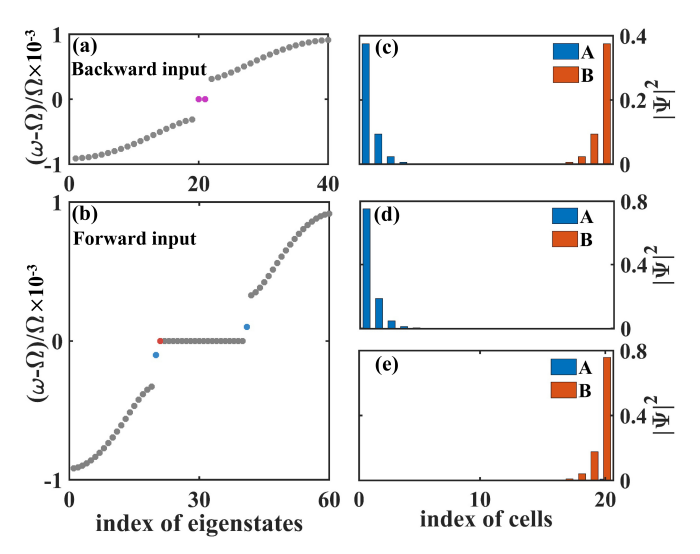


FIG. 3. Nonreciprocal energy spectra (a, b) and probability distribution (c-e). (a) and (c) for the  $CCW_A - CW_B$  supermode without coupling to the QEs, g = 0. (b), (d), and (e) for the  $CW_A - CCW_B$  supermode with coupling to the QEs,  $g/\Omega = 10^{-4}$ . Other parameters are  $J_1/\Omega = 3 \times 10^{-4}$ ,  $J_2 = 2J_1$ .

become wider, see Fig. 2(c). Interestingly, these two band gaps possess very peculiar SPESs. These SPESs are very different from the backward case.

Figure 3 shows energy spectra of a finite unit cell with N = 20 and the probability distribution corresponding to the SPESs in the two oppositely circulating supermodes of the system. As for the  $CCW_A - CW_B$  supermode without coupling to the QEs, there are 2N eigenvalues and two degenerate zero-energy SPESs falling in the bulk band gap [see the purple asterisks in Fig. 3(a)]. The wave functions of two edge states localize at the left or right boundary and exponentially decay from the boundaries [see Fig. 3(c)].

In stark contrast, when the system is excited in the  $CW_A$  –  $CCW_B$  supermode, the coupling to the QEs results in N more eigenvalues. Due to the coupling with the QEs, the left SPES becomes doublet, forming two superstates of the  $R_A$  set and the QEs with an energy splitting proportional to the coupling strength g [60, 66, 67], see the dashed black curves in Fig. 2(c). As an example, the energy spectrum of the QE-CROW system with N = 20 and  $g/\Omega = 10^{-4}$  is shown in Fig. 3(c). The left SPESs have eigenenergies at  $\omega - \Omega = \pm g$ (see the blue asterisks). In Fig. 3(d), the probability of the A sublattice includes the contribution of the QE. Unlike the SPESs of the  $CCW_A - CW_B$  supermode, the wave functions of these SPESs only localize on the left edge of the system with an exponentially decaying probability distribution at the sites of both the A-sublattice resonator and the QE. The right zeroenergy SPES still exists, [see the red asterisk in Fig. 3(b)], because the R<sub>B</sub> resonators decouple from the QE. The wave function of this right SPES localizes at the right boundary [see Fig. 3(e)]. The nonreciprocal SPESs is the unique property of our chiral QE-CROW system.

For small N, the left and right SPESs overlap in the backward-input case because of their exponentially decaying

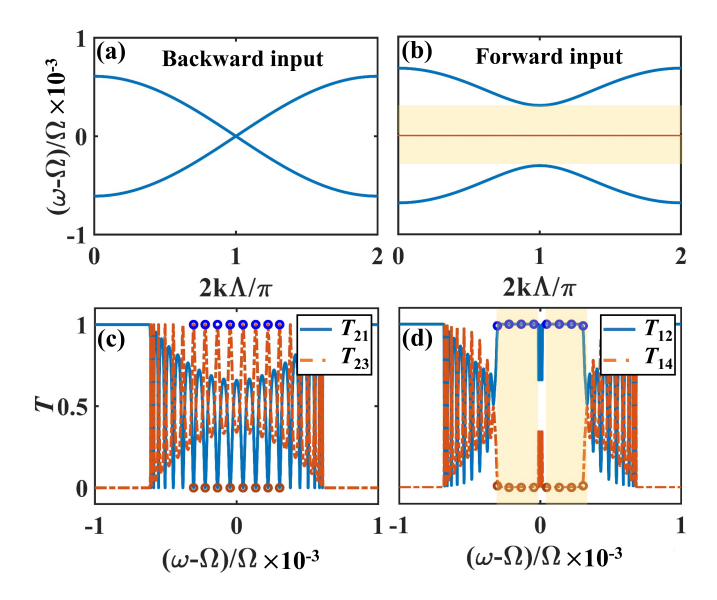


FIG. 4. Single-photon band structure (a, b) and transmission (c, d) with N=10 for  $J_1=J_2$ . In (a, c) the  $CCW_A-CW_B$  supermode is excited, and g=0. In (b, d) the  $CW_A-CCW_B$  supermode is driven, and  $g/\Omega=3\times10^{-4}$ . Other parameters are  $J_1/\Omega=3\times10^{-4}$ ,  $J_2=J_1$ .

distribution. This wavefunction overlap at zero-energy frequency results in a SPES tunneling. In contrast, in the forward case, this SPES-overlap induced tunneling is greatly suppressed because the left and right SPESs are nondegenerate in energy. Therefore, we can realize a single-photon circulator via the nonreciprocal SPESs with few unit cells [60].

Nonreciprocal single-photon band gap.—The case  $J_1 > J_2$  opens a band gap but exhibits trivial physical properties. We are not interested in it here. Now we discuss the case  $J_1 = J_2$ . Figures 4(a,b) show a nonreciprocal single-photon band gap for oppositely propagating photons. For the backward input, the two bands are closed and thus form continuous conduction bands. In comparison, as in the case of  $J_1 < J_2$ , the  $CW_A - CCW_B$  supermode also exhibits two band gaps, separated by a flat band due to the interaction with QEs, see the yellow region in Fig. 4(b). The band gap increases with the QE-resonator coupling strength, permitting a wider nonreciprocal bandwidth. This nonreciprocal single-photon band gap allows to conduct single-photon circulators. The same results can be derived by using the transfer matrix method [60].

The band structures of our system characterize the transmission of single photons. When we consider the case with finite unit cells in the 1D CROW, the conduction band region turns into transmission peaks. Using Eqs. (6), we calculate the transmission spectrum of our QE-CROW system with N=10 in the two opposite-propagation cases. For single photons input to port 2, see Fig. 4(c), the excited CCW<sub>A</sub> – CW<sub>B</sub> supermode decouples from the QEs. This system is equivalent to the conventional CROW without QEs. There are 2N peaks in the transmission  $T_{23}$  and dips in  $T_{21}$ . In contrast, when the single-photon wave packet inputs to port 1, the transmission  $T_{14}$  is zero, because the photon transport is forbidden in the band gap, and thus  $T_{12}=1$ , see Fig. 4(d). Clearly, we obtain *strong nonreciprocity in the transmission* at the frequen-

cies corresponding to the peaks of  $T_{23}$ , where  $T_{23} \approx 1$ , or the dips of  $T_{21}$ , where  $T_{21} \approx 0$ . For  $g/\Omega = 3 \times 10^{-4}$ , we have eight nonreciprocal frequency windows at  $(\omega - \Omega)/\Omega \approx \{\pm 30, \pm 22, \pm 13, \pm 4.5\} \times 10^{-5}$ , see blue circles. Due to the symmetry of the CROW, we obtain  $T_{12} = T_{34}$  and  $T_{23} = T_{41}$ . Thus, we can choose any one of eight frequencies in the bandgap region to achieve  $T_{23} = 1$  ( $T_{21} = 0$ ). In this case, we can attain a frequency-multiplex single-photon circulator with a circling photon transport direction  $1 \rightarrow 2 \rightarrow 3 \rightarrow 4 \rightarrow 1$  at frequencies marked by circles in Figs. 4(d).

Note that this single-photon circulator is robust against backscattering (see the Supplemental Material [60]). The chiral coupling between the QE and the vacuum field of  $R_A$  eigenmodes induces an extra phase shift  $Re[\varphi]$  for the CW mode, shifting its resonance frequency and leading to non-degenerate with the CCW mode. Thus, the opposite CW mode excited by a backscattering of a propagating CCW mode is forbidden in the nonreciprocal band gap, see Figs. 4 (a,b). Our chiral QE-CROW system promises a new type of backscattering-immune optical device.

Implementation.—The required 1D CROW can be made with silicon oxynitride [68], silicon on insulator [69, 70] or lithium niobium oxynitride [71]. We consider a QE-CROW system consisting of N = 10 resonators with a radius of  $r = 40 \mu \text{m}$  and  $n_{\text{eff}} = 2$ , yielding  $\mathcal{F}/2\pi = 0.6 \text{ THz}$ . The external dissipations of resonators can be calculated as  $\gamma_{\rm ex}/2\pi = 19.4$  GHz [setting  $\gamma_{\rm in} = 0.02\gamma_{\rm ex}$ , thus  $\gamma_{\rm tol}/2\pi =$  $(\gamma_{\rm ex} + \gamma_{\rm in})/2\pi = 19.8$  GHz] [61]. For the coupling coefficient  $\kappa_1 = \kappa_2 = 0.1i$ , the coupling strength between resonators can be deduced as  $J_1/\gamma_{\text{tol}} = J_2/\gamma_{\text{tol}} = 3$ . We take  $\Omega/2\pi =$ 195 THz. Regarding QEs, we choose  $\lambda = 1.538 \,\mu\text{m}$  [72–74] so that  $\omega_q = \Omega$  and a dipole moment of  $|\mathbf{d}| = 20$  Debye [75], yielding  $\gamma = 2\pi \times 5.48$  MHz, and  $g/\gamma_{tol} = 0.77$  for a resonator mode volume of  $V_{\rm m}=2.0~\mu{\rm m}^3$  [31, 76]. The chiral QElight interaction can be optically induced as aforementioned. The fidelity and the average photon survival probability of the circulator are calculated as {0.99, 0.98} at two optimal frequency windows  $(\omega - \Omega)/\Omega \approx \pm 4.5 \times 10^{-5}$  [10, 25]. Moreover, we achieve a nonreciprocal transmission bandwidth of  $\sim 2\pi \times 2.4$  GHz and an average insertion loss of 1.12 dB for a circulator fidelity larger than 0.95. Thus, the nonreciprocal SPES and high-performance single-photon circulator can be achieved even in the weak coupling regime  $g < \gamma_{\text{tol}}$ . In stark contrast, a conventional chiral quantum optics system using a single resonator can achieve the single-photon diode and circulator only in the strong coupling regime [24–26, 31]. Thus, our proposal greatly relaxes its experimental challenge.

Conclusion.—We have shown that nonreciprocal single-photon band structures can be achieved in a chiral QE-CROW system. The chiral QE-CROW system with a nonreciprocal band gap can construct frequency-multiplex single-photon circulators. Our work extends photonic band structures of periodic photonic structures to exhibit remarkable magnetic-free quantum nonreciprocity, likely beyond condensed matter.

K.X. and Y.L thank Prof. Haiqing Lin for his stimulating and constructive discussion. J.T. thanks Chaohua Wu for helpful discussions. Y.L. and K.X. are supported by the National Key R&D Program of China (Grants

No. 2019YFA0308700, No. 2017YFA0303703, and No. 2017YFA0303701), the National Natural Science Foundation of China (Grants No. 11874212 and No. 11890704), the Fundamental Research Funds for the Central Universities (Grant No. 021314380095), the Program for Innovative Talents and Entrepreneurs in Jiangsu, and the Excellent Research Program of Nanjing University (Grant No. ZYJH002). W.N is supported by the National Natural Science Foundation of China (Grants No. 11690031). F.N. is supported by the Nippon Telegraph and Telephone Corporation (NTT) Research, the Japan Science and Technology Agency (JST) [via the Quantum Leap Flagship Program (Q-LEAP), the Moonshot R&D Grant Number JPMJMS2061, and the Centers of Research

Excellence in Science and Technology (CREST) Grant No. JPMJCR1676], the Japan Society for the Promotion of Science (JSPS) [via the Grants-in-Aid for Scientific Research (KAKENHI) Grant No. JP20H00134 and the JSPS-RFBR Grant No. JPJSBP120194828], the Army Research Office (ARO) (Grant No. W911NF-18-1-0358), the Asian Office of Aerospace Research and Development (AOARD) (via Grant No. FA2386-20-1-4069), and the Foundational Questions Institute Fund (FQXi) via Grant No. FQXi-IAF19-06. We thank the High Performance Computing Center of Nanjing University for allowing the numerical calculations on its blade cluster system.

- [1] H. J. Kimble, The quantum internet, Nature (London) 453, 1023 (2008).
- [2] Z. Lin, H. Ramezani, T. Eichelkraut, T. Kottos, H. Cao, and D. N. Christodoulides, Unidirectional invisibility induced by PT-symmetric periodic structures, Phys. Rev. Lett. 106, 213901 (2011).
- [3] Ş. K. Özdemir, S. Rotter, F. Nori, and L. Yang, Parity-time symmetry and exceptional points in photonics, Nat. Mater. 18, 783 (2019).
- [4] D. Jalas, A. Petrov, M. Eich, W. Freude, S. Fan, Z. Yu, R. Baets, M. Popović, A. Melloni, J. D. Joannopoulos, M. Vanwolleghem, C. R. Doerr, and H. Renner, What is—and what is not—an optical isolator, Nat. Photonics 7, 579 (2013).
- [5] B. Bahari, A. Ndao, F. Vallini, A. El Amili, Y. Fainman, and B. Kanté, Nonreciprocal lasing in topological cavities of arbitrary geometries, Science 358, 636 (2017).
- [6] Y. Jiang, S. Maayani, T. Carmon, F. Nori, and H. Jing, Nonreciprocal phonon laser, Phys. Rev. Appl. 10, 064037 (2018).
- [7] B. Peng, Ş. K. Özdemir, F. Lei, F. Monifi, M. Gianfreda, G. L. Long, S. Fan, F. Nori, C. M. Bender, and L. Yang, Parity-time-symmetric whispering-gallery microcavities, Nat. Phys. 10, 394 (2014).
- [8] Q.-T. Cao, H. Wang, C.-H. Dong, H. Jing, R.-S. Liu, X. Chen, L. Ge, Q. Gong, and Y.-F. Xiao, Experimental demonstration of spontaneous chirality in a nonlinear microresonator, Phys. Rev. Lett. 118, 033901 (2017).
- [9] S. Zhang, Y. Hu, G. Lin, Y. Niu, K. Xia, J. Gong, and S. Gong, Thermal-motion-induced non-reciprocal quantum optical system, Nat. Photonics 12, 744 (2018).
- [10] K. Xia, F. Nori, and M. Xiao, Cavity-free optical isolators and circulators using a chiral cross-Kerr nonlinearity, Phys. Rev. Lett. 121, 203602 (2018).
- [11] P. Yang, X. Xia, H. He, S. Li, X. Han, P. Zhang, G. Li, P. Zhang, J. Xu, Y. Yang, and T. Zhang, Realization of nonlinear optical nonreciprocity on a few-photon level based on atoms strongly coupled to an asymmetric cavity, Phys. Rev. Lett. 123, 233604 (2019).
- [12] E.-Z. Li, D.-S. Ding, Y.-C. Yu, M.-X. Dong, L. Zeng, W.-H. Zhang, Y.-H. Ye, H.-Z. Wu, Z.-H. Zhu, W. Gao, G.-C. Guo, and B.-S. Shi, Experimental demonstration of cavity-free optical isolators and optical circulators, Phys. Rev. Res. 2, 033517 (2020).
- [13] L. Tang, J. Tang, H. Wu, J. Zhang, M. Xiao, and K. Xia, Broad-intensity-range optical nonreciprocity based on feedback-induced Kerr nonlinearity, Photonics Res. 9, 1218 (2021).

- [14] L. Tang, J. Tang, M. Chen, F. Nori, M. Xiao, and K. Xia, Quantum squeezing induced optical nonreciprocity, arXiv:2110.05016 [quant-ph] (2021).
- [15] M. Hafezi and P. Rabl, Optomechanically induced non-reciprocity in microring resonators, Opt. Express 20, 7672 (2012).
- [16] Z. Shen, Y.-L. Zhang, Y. Chen, C.-L. Zou, Y.-F. Xiao, X.-B. Zou, F.-W. Sun, G.-C. Guo, and C.-H. Dong, Experimental realization of optomechanically induced non-reciprocity, Nat. Photonics 10, 657 (2016).
- [17] F. Ruesink, M.-A. Miri, A. Alù, and E. Verhagen, Nonreciprocity and magnetic-free isolation based on optomechanical interactions, Nat. Commun. 7, 13662 (2016).
- [18] S. Maayani, R. Dahan, Y. Kligerman, E. Moses, A. U. Hassan, H. Jing, F. Nori, D. N. Christodoulides, and T. Carmon, Flying couplers above spinning resonators generate irreversible refraction, Nature (London) 558, 569 (2018).
- [19] R. Huang, A. Miranowicz, J.-Q. Liao, F. Nori, and H. Jing, Nonreciprocal photon blockade, Phys. Rev. Lett. 121, 153601 (2018).
- [20] D.-W. Wang, H.-T. Zhou, M.-J. Guo, J.-X. Zhang, J. Evers, and S.-Y. Zhu, Optical diode made from a moving photonic crystal, Phys. Rev. Lett. 110, 093901 (2013).
- [21] S. A. R. Horsley, J.-H. Wu, M. Artoni, and G. C. La Rocca, Optical nonreciprocity of cold atom Bragg mirrors in motion, Phys. Rev. Lett. 110, 223602 (2013).
- [22] D. L. Sounas and A. Alù, Non-reciprocal photonics based on time modulation, Nat. Photonics 11, 774 (2017).
- [23] C. Sayrin, C. Junge, R. Mitsch, B. Albrecht, D. O'Shea, P. Schneeweiss, J. Volz, and A. Rauschenbeutel, Nanophotonic optical isolator controlled by the internal state of cold atoms, Phys. Rev. X 5, 041036 (2015).
- [24] K. Xia, G. Lu, G. Lin, Y. Cheng, Y. Niu, S. Gong, and J. Twamley, Reversible nonmagnetic single-photon isolation using unbalanced quantum coupling, Phys. Rev. A 90, 043802 (2014).
- [25] M. Scheucher, A. Hilico, E. Will, J. Volz, and A. Rauschenbeutel, Quantum optical circulator controlled by a single chirally coupled atom, Science 354, 1577 (2016).
- [26] P. Lodahl, S. Mahmoodian, S. Stobbe, A. Rauschenbeutel, P. Schneeweiss, J. Volz, H. Pichler, and P. Zoller, Chiral quantum optics, Nature (London) 541, 473 (2017).
- [27] M. J. Mehranad, A. P. Foster, R. Dost, E. Clarke, P. K. Patil, A. M. Fox, M. S. Skolnick, and L. R. Wilson, Chiral topological photonics with an embedded quantum emitter, Optica 7, 1690

- (2020).
- [28] M.-X. Dong, K. Xia, W.-H. Zhang, Y.-C. Yu, Y.-H. Ye, E.-Z. Li, L. Zeng, D.-S. Ding, B.-S. Shi, G.-C. Guo, and F. Nori, Alloptical reversible single-photon isolation at room temperature, Sci. Adv. 7, eabe8924 (2021).
- [29] X.-X. Hu, Z.-B. Wang, P. Zhang, G.-J. Chen, Y.-L. Zhang, G. Li, X.-B. Zou, T. Zhang, H. X. Tang, C.-H. Dong, G.-C. Guo, and C.-L. Zou, Noiseless photonic non-reciprocity via optically-induced magnetization, Nat. Commun. 12, 2389 (2021).
- [30] S. Pucher, C. Liedl, S. Jin, A. Rauschenbeutel, and P. Schneeweiss, Atomic spin-controlled non-reciprocal raman amplification of fibre-guided light, arXiv preprint arXiv:2107.07272 (2021).
- [31] L. Tang, J. Tang, W. Zhang, G. Lu, H. Zhang, Y. Zhang, K. Xia, and M. Xiao, On-chip chiral single-photon interface: Isolation and unidirectional emission, Phys. Rev. A 99, 043833 (2019).
- [32] T. Ramos, H. Pichler, A. J. Daley, and P. Zoller, Quantum spin dimers from chiral dissipation in cold-atom chains, Phys Rev Lett 113, 237203 (2014).
- [33] I. Söllner, S. Mahmoodian, S. L. Hansen, L. Midolo, A. Javadi, G. Kiršanskė, T. Pregnolato, H. El-Ella, E. H. Lee, J. D. Song, S. Stobbe, and P. Lodahl, Deterministic photon-emitter coupling in chiral photonic circuits, Nat. Nanotechnol. 10, 775 (2015).
- [34] T. Li, Z. Gao, and K. Xia, Nonlinear-dissipation-induced nonreciprocal exceptional points, Opt. Express 29, 17613 (2021).
- [35] J. Tang, L. Tang, H. Wu, Y. Wu, H. Sun, H. Zhang, T. Li, Y. Lu, M. Xiao, and K. Xia, Towards on-demand heralded single-photon sources via photon blockade, Phys. Rev. Appl. 15, 064020 (2021).
- [36] D. Roy, C. M. Wilson, and O. Firstenberg, Colloquium: Strongly interacting photons in one-dimensional continuum, Rev. Mod. Phys. 89, 021001 (2017).
- [37] D. E. Chang, J. S. Douglas, A. González-Tudela, C.-L. Hung, and H. J. Kimble, Colloquium: Quantum matter built from nanoscopic lattices of atoms and photons, Rev. Mod. Phys. 90, 031002 (2018).
- [38] A. Yariv, Y. Xu, R. K. Lee, and A. Scherer, Coupled-resonator optical waveguide: a proposal and analysis, Opt. Lett. 24, 711 (1999).
- [39] J. K. S. Poon, J. Scheuer, S. Mookherjea, G. T. Paloczi, Y. Huang, and A. Yariv, Matrix analysis of microring coupledresonator optical waveguides, Opt. Express 12, 90 (2004).
- [40] J. Perczel, J. Borregaard, D. E. Chang, S. F. Yelin, and M. D. Lukin, Topological quantum optics using atomlike emitter arrays coupled to photonic crystals, Phys. Rev. Lett. 124, 083603 (2020).
- [41] Y. Ao, X. Hu, Y. You, C. Lu, Y. Fu, X. Wang, and Q. Gong, Topological phase transition in the non-Hermitian coupled resonator array, Phys. Rev. Lett. 125, 013902 (2020).
- [42] J. Li, B. Gao, C. Zhu, J. Xu, and Y. Yang, Nonreciprocal photonic composited Su-Schrieffer-Heeger chain, Appl. Phys. Lett. 119, 141108 (2021).
- [43] K. Fang, Z. Yu, and S. Fan, Microscopic theory of photonic one-way edge mode, Phys. Rev. B **84**, 075477 (2011).
- [44] L. Lu, J. D. Joannopoulos, and M. Soljačió, Topological photonics, Nat. Photonics 8, 821 (2014).
- [45] A. B. Khanikaev and G. Shvets, Two-dimensional topological photonics, Nat. Photonics 11, 763 (2017).
- [46] T. Ozawa, H. M. Price, A. Amo, N. Goldman, M. Hafezi, L. Lu, M. C. Rechtsman, D. Schuster, J. Simon, O. Zilberberg, and I. Carusotto, Topological photonics, Rev. Mod. Phys. 91, 015006 (2019).

- [47] X. Xi, J. Ma, S. Wan, C.-H. Dong, and X. Sun, Observation of chiral edge states in gapped nanomechanical graphene, Sci. Adv. 7, eabe 1398 (2021).
- [48] K. Y. Bliokh and F. Nori, Characterizing optical chirality, Phys. Rev. A 83, 021803 (2011).
- [49] K. Y. Bliokh, A. Y. Bekshaev, and F. Nori, Extraordinary momentum and spin in evanescent waves, Nat. Commun. 5, 3300 (2014).
- [50] K. Y. Bliokh, D. Smirnova, and F. Nori, Quantum spin Hall effect of light, Science 348, 1448 (2015).
- [51] F. Alpeggiani, K. Y. Bliokh, F. Nori, and L. Kuipers, Electromagnetic helicity in complex media, Phys. Rev. Lett. 120, 243605 (2018).
- [52] J. K. S. Poon, J. Scheuer, Y. Xu, and A. Yariv, Designing coupled-resonator optical waveguide delay lines, J. Opt. Soc. Am. B 21, 1665 (2004).
- [53] J. D. Thompson, T. G. Tiecke, N. P. de Leon, J. Feist, A. V. Akimov, M. Gullans, A. S. Zibrov, V. Vuletić, and M. D. Lukin, Coupling a single trapped atom to a nanoscale optical cavity, Science 340, 1202 (2013).
- [54] S. Barik, A. Karasahin, C. Flower, T. Cai, H. Miyake, W. De-Gottardi, M. Hafezi, and E. Waks, A topological quantum optics interface, Science 359, 666 (2018).
- [55] J. Yang, C. Qian, X. Xie, K. Peng, S. Wu, F. Song, S. Sun, J. Dang, Y. Yu, S. Shi, J. He, M. J. Steer, I. G. Thayne, B.-B. Li, F. Bo, Y.-F. Xiao, Z. Zuo, K. Jin, C. Gu, and X. Xu, Diabolical points in coupled active cavities with quantum emitters, Light-Sci. Appl. 9, 6 (2020).
- [56] A. Branny, S. Kumar, R. Proux, and B. D. Gerardot, Deterministic strain-induced arrays of quantum emitters in a two-dimensional semiconductor, Nat. Commun. 8, 15053 (2017).
- [57] C. Palacios-Berraquero, D. M. Kara, A. R. P. Montblanch, M. Barbone, P. Latawiec, D. Yoon, A. K. Ott, M. Loncar, A. C. Ferrari, and M. Atatüre, Large-scale quantum-emitter arrays in atomically thin semiconductors, Nat. Commun. 8, 15093 (2017).
- [58] W. P. Su, J. R. Schrieffer, and A. J. Heeger, Solitons in polyacetylene, Phys. Rev. Lett. 42, 1698 (1979).
- [59] Z.-Q. Jiao, S. Longhi, X.-W. Wang, J. Gao, W.-H. Zhou, Y. Wang, Y.-X. Fu, L. Wang, R.-J. Ren, L.-F. Qiao, and X.-M. Jin, Experimentally detecting quantized Zak phases without chiral symmetry in photonic lattices, Phys. Rev. Lett. 127, 147401 (2021).
- [60] See Supplemental Material for the detailed derivation.
- [61] J. Tang, L. Tang, and K. Xia, Single-photon transport in a whispering-gallery mode microresonator directionally coupled with a two-level quantum emitter, arXiv preprint arXiv:2110.09375 (2021).
- [62] J. K. Asbóth, L. Oroszlány, and A. Pályi, A short course on topological insulators, Lecture notes in physics 919, 166 (2016).
- [63] M. F. Yanik, W. Suh, Z. Wang, and S. Fan, Stopping light in a waveguide with an all-optical analog of electromagnetically induced transparency, Phys. Rev. Lett. 93, 233903 (2004).
- [64] P. Wang, Y. Zheng, X. Chen, C. Huang, Y. V. Kartashov, L. Torner, V. V. Konotop, and F. Ye, Localization and delocalization of light in photonic moiré lattices, Nature (London) 577, 42 (2020).
- [65] Y. He, R. Mao, H. Cai, J.-X. Zhang, Y. Li, L. Yuan, S.-Y. Zhu, and D.-W. Wang, Flat-band localization in Creutz superradiance lattices, Phys. Rev. Lett. 126, 103601 (2021).
- [66] Y. Peng, Y. Bao, and F. von Oppen, Boundary Green functions of topological insulators and superconductors, Phys. Rev. B 95, 235143 (2017).

- [67] V. M. Martinez Alvarez and M. D. Coutinho-Filho, Edge states in trimer lattices, Phys. Rev. A 99, 013833 (2019).
- [68] C. F. Andrea Melloni, Francesco Morichetti and M. Martinelli, Continuously tunable 1 byte delay in coupled-resonator optical waveguides, Opt. Lett. 33, 2389 (2008).
- [69] M. Hafezi, S. Mittal, J. Fan, A. Migdall, and J. M. Taylor, Imaging topological edge states in silicon photonics, Nat. Photonics 7, 1001 (2013).
- [70] J. Wang, Z. Yao, and A. W. Poon, Silicon-nitride-based integrated optofluidic biochemical sensors using a coupled-resonator optical waveguide, Front. Mater. 2, 10.3389/fmats.2015.00034 (2015).
- [71] M. Wang, N. Yao, R. Wu, Z. Fang, S. Lv, J. Zhang, J. Lin, W. Fang, and Y. Cheng, Strong nonlinear optics in on-chip coupled lithium niobate microdisk photonic molecules, New J. Phys. 22, 073030 (2020).
- [72] A. Kors, J. P. Reithmaier, and M. Benyoucef, Telecom wave-

- length single quantum dots with very small excitonic fine-structure splitting, Appl. Phys. Lett. **112**, 172102 (2018).
- [73] S. Haffouz, K. D. Zeuner, D. Dalacu, P. J. Poole, J. Lapointe, D. Poitras, K. Mnaymneh, X. Wu, M. Couillard, M. Korkusinski, E. Schöll, K. D. Jöns, V. Zwiller, and R. L. Williams, Bright single inasp quantum dots at telecom wavelengths in positioncontrolled inp nanowires: The role of the photonic waveguide, Nano Lett. 18, 3047 (2018).
- [74] Y. Arakawa and M. J. Holmes, Progress in quantum-dot single photon sources for quantum information technologies: A broad spectrum overview, Appl. Phys. Rev. **7**, 021309 (2020).
- [75] H. Htoon, T. Takagahara, D. Kulik, O. Baklenov, A. L. Holmes, and C. K. Shih, Interplay of rabi oscillations and quantum interference in semiconductor quantum dots, Phys. Rev. Lett. 88, 087401 (2002).
- [76] Q. Xu, D. Fattal, and R. G. Beausoleil, Silicon microring resonators with 1.5-μm radius, Opt. Express 16, 4309 (2008).

# Supplemental material for "Nonreciprocal single-photon band structure"

Jiangshan Tang,<sup>1,2</sup> Wei Nie,<sup>3</sup> Lei Tang,<sup>1</sup> Mingyuan Chen,<sup>1</sup>
Xin Su,<sup>1,4</sup> Yanqing Lu,<sup>1,2</sup> Franco Nori,<sup>3,5</sup> and Keyu Xia<sup>1,2,6\*</sup>

<sup>1</sup>College of Engineering and Applied Sciences, National Laboratory of Solid State Microstructures, and Collaborative Innovation Center of Advanced Microstructures, Nanjing University, Nanjing 210023, China

<sup>2</sup>School of Physics, Nanjing University, Nanjing 210023, China

<sup>3</sup> RIKEN Quantum Computing Center, RIKEN Cluster for Pioneering Research, Wako-shi, Saitama 351-0198, Japan

<sup>4</sup>School of Electronic Science and Engineering, Nanjing University, Nanjing 210023, China

<sup>5</sup> Physics Department, The University of Michigan, Ann Arbor, Michigan 48109-1040, USA

<sup>6</sup>Jiangsu Key Laboratory of Artificial Functional Materials, Nanjing University, Nanjing 210023, China

In this supplemental material, we derive the recursive boundary Green function and provide a detailed derivation of the transfer matrix method. We show that the property of non-reciprocal single-photon edge states in our system can be used to construct a single-photon circulator. We also exhibit that the single-photon transmission is immune to the backscattering in the non-reciprocal single-photon band gap, and discuss the effect of the number of unit cells on frequency-multiplexing channels of the single-photon circulator.

#### I. RECURSIVE BOUNDARY GREEN FUNCTION

Here we study the localization properties of edge states and their relationship with the coupling strengths,  $\{g, J_1, J_2\}$ , when our system is excited in the  $CW_A - CCW_B$  supermode (forward input). In this case, our QE-CROW system is equivalent to an L-type trimer chain with each unit cell containing three sites, the QE, the A-sublattice resonator, and the B-sublattice resonator. The QE is only coupled with the A-sublattice resonator. We divide the unit cell into A and B sublattice groups, where the A sublattice contains the A-sublattice resonator and the QE, and the B sublattice only involves the B-sublattice resonator. Therefore, this L-type trimer chain can be treated as an SSH-like model. We use the recursive boundary Green function method to link the existence of edge states with the fixed points of the recursion [1, 2]. Hereafter, we consider the case  $J_1 < J_2$ , which corresponds to the situation with edge states. In contrast, there are no edge states in the opposite case, i.e.,  $J_1 \ge J_2$ .

Following the calculation steps in Ref. [1], we can relate the boundary Green function  $G_N$  of this SSH-like chain with N unit cells to the boundary Green function  $G_{N-1}$  of a chain with (N-1) unit cells and write the Dyson equation:

$$\left(\epsilon_N^{-1} - V_{N-1}G_{N-1}V_{N-1}^{\dagger}\right)G_N = \mathbb{I} , \qquad (S1)$$

where  $\epsilon_N^{-1} = \mathbb{I}\omega - h_N$  is the bare Green function of the Nth unit cell and  $V_{N-1}$  is correlated with coupling strengths  $\{g, J_1, J_2\}$ . To prove that our system has edge states located at the left boundary of the chain, we consider the left boundary Green function and obtain

$$\epsilon_n^{-1} = \begin{cases} \mathbb{I}\omega & n = 2N - 1\\ \begin{pmatrix} \omega & -g\\ -g & \omega \end{pmatrix} & n = 2N \end{cases}, \qquad V_n = \begin{cases} \begin{pmatrix} 0\\ J_1 \end{pmatrix} & n = 2N - 1\\ J_2 & n = 2N \end{cases}$$
(S2)

from Eq. (1) in the main text. By iterating the recursion Eq. (S1) from the left boundary, we can obtain a recursion for the 2Nth and the (2N-1)th cells,

$$\left[ \begin{pmatrix} \omega & -g \\ -g & \omega \end{pmatrix} - \begin{pmatrix} 0 \\ J_1 \end{pmatrix} G_{2N-1}^L \begin{pmatrix} 0 & J_1 \end{pmatrix} \right] G_{2N}^L = \mathbb{I} ,$$
(S3a)

$$\begin{bmatrix} \begin{pmatrix} \omega & 0 \\ 0 & \omega \end{pmatrix} - J_2^2 G_{2N-2}^L \end{bmatrix} G_{2N-1}^L = \mathbb{I} , \qquad (S3b)$$

respectively. Here,  $G_{2N}^L$  and  $G_{2N-2}^L$  take the form of a  $2 \times 2$  matrix,

$$G_{2N}^{L} = \begin{pmatrix} G_{11}^{2N} & G_{12}^{2N} \\ G_{21}^{2N} & G_{22}^{2N} \end{pmatrix}, \quad G_{2N-2}^{L} = \begin{pmatrix} G_{11}^{2N-2} & G_{12}^{2N-2} \\ G_{21}^{2N-2} & G_{22}^{2N-2} \end{pmatrix}.$$
 (S4)

Substituting Eq. (S4) into Eqs. (S3), we obtain

$$\left(\omega - J_2^2 G_{11}^{2N-2}\right) G_{2N-1}^L = 1 \,, \tag{S5a}$$

$$G_{11}^{2N} \left(\omega^2 - \omega J_1^2 G_{2N-1}^L - g^2\right) - \left(\omega - J_1^2 G_{2N-1}^L\right) = 0.$$
 (S5b)

Then we have

$$G_{11}^{2N} = \frac{\omega \left(\omega - J_2^2 G_{11}^{2N-2}\right) - J_1^2}{\left(\omega^2 - g^2\right) \left(\omega - J_2^2 G_{11}^{2N-2}\right) - J_1^2 \omega} . \tag{S6}$$

In order to analyze the recursion, we further write it as

$$G_{11}^{2N} - G_{11}^{2N-2} = \xi_L \left( G_{11}^{2N-2} \right), \tag{S7}$$

where the function  $\xi_L(x)$  is defined as

$$\xi_L(x) = \frac{\omega(\omega - J_2^2 x) - J_1^2}{(\omega^2 - g^2)(\omega - J_2^2 x) - J_1^2 \omega} - x.$$
 (S8)

The fixed-point boundary Green functions can be obtained by solving the zeros of the function  $\xi_L(x)$ . We can write the solution for Eq. S8 as follows:

$$x = \frac{\omega(\omega^2 - g^2 + J_2^2 - J_1^2) \pm \sqrt{\omega^2(\omega^2 - g^2 + J_2^2 - J_1^2)^2 - 4J_2^2(\omega^2 - g^2)(\omega^2 - J_1^2)}}{2J_2^2(\omega^2 - g^2)},$$
 (S9)

and expand in power series of  $(\omega \pm g)$ ,

$$G_{\text{reg}}^{L} = \pm \frac{J_1^2 - 4g^2 - J_2^2}{8gJ_2^2} + O(\omega \pm g),$$
 (S10)

$$G_{\text{sing}}^{L} = \frac{J_2^2 - J_1^2}{2J_2^2 (\omega \pm g)} \pm \frac{J_1^2 - 4g^2 - J_2^2}{8gJ_2^2} + O(\omega \pm g). \tag{S11}$$

The above fixed-point boundary Green functions characterize the absence and presence of edge states localized on the left boundary of the chain. Corresponding to the edge state, the band-gap state makes the boundary Green function singular for  $\omega \pm g$ , see Eq. (S11). In contrast, when the boundary Green function is regular [corresponding to Eq. (S10)], there are no edge states. Further, when  $\xi'_L(x) < 0$ , it holds a stable fixed point, thus we have

$$\left. \frac{\partial \xi_L \left( G_{\text{sing}}^L \right)}{\partial x} \right|_{\omega = \pm q} = \frac{J_1^2}{J_2^2} - 1 < 0. \tag{S12}$$

We can find that only when  $|J_1| < |J_2|$ , the fixed point is stable, which means that there are edge states localized at the left boundary of the chain.

Similarly, when we consider the right boundary Green function, we have:

$$\epsilon_n^{-1} = \begin{cases} \begin{pmatrix} \omega & -g \\ -g & \omega \end{pmatrix} & n = 2N - 1 \\ \mathbb{I}\omega & n = 2N \end{cases}, \qquad V_n = \begin{cases} \begin{pmatrix} J_1 & 0 \end{pmatrix} & n = 2N - 1 \\ J_2 & n = 2N \end{cases}.$$
 (S13)

With the same calculation procedure, we can derive the iterative relation:

$$G_{2N}^{R} = \left\{ \omega - J_1^2 \left[ \left( \omega - J_2^2 G_{2N-2}^R \right)^2 - g^2 \right]^{-1} \right\}^{-1} . \tag{S14}$$

We now rewrite the recursion Eq. (S14) as

$$G_{2N}^R - G_{2N-2}^R = \xi_R(G_{2N-2}^R),$$
 (S15)

with

$$\xi_R(x) = \left\{ \omega - J_1^2 \left[ \left( \omega - J_2^2 x \right)^2 - g^2 \right]^{-1} \right\}^{-1} - x . \tag{S16}$$

The fixed-point boundary Green function can be obtained by seeking the zeros of Eq. (S16), that is

$$\omega J_2^4 x^3 - (2\omega^2 J_2^2 + J_2^4) x^2 + \left[\omega \left(\omega^2 - g^2 + 2J_2^2\right) - J_1^2\right] x + g^2 - \omega^2 = 0.$$
 (S17)

The singularity of the solution of Eq. (S17) characterizes the existence of edge states. For this cubic equation, using the famous Cardano formula, we can find that a singularity only appears at  $\omega = 0$ . Therefore, this means that there is a right edge state at zero energy. Indeed, under the condition of  $J_1 < J_2$ , the presence of edge states at zero energy is a characteristic of this SSH-like chain. Unlike the left edge state, its energy remain unchanged because the B-sublattice resonator is not coupled with the QE.

### II. THE TRANSFER MATRIX FORMALISM OF OUR CHIRAL QE-CROW SYSTEM

We derive the transfer matrix formalism to treat the dynamics of our chiral QE-CROW system. We find that the single-photon dispersion relations solved by the transfer matrix are consistent with the results obtained by solving the Hamiltonian directly in the main text.

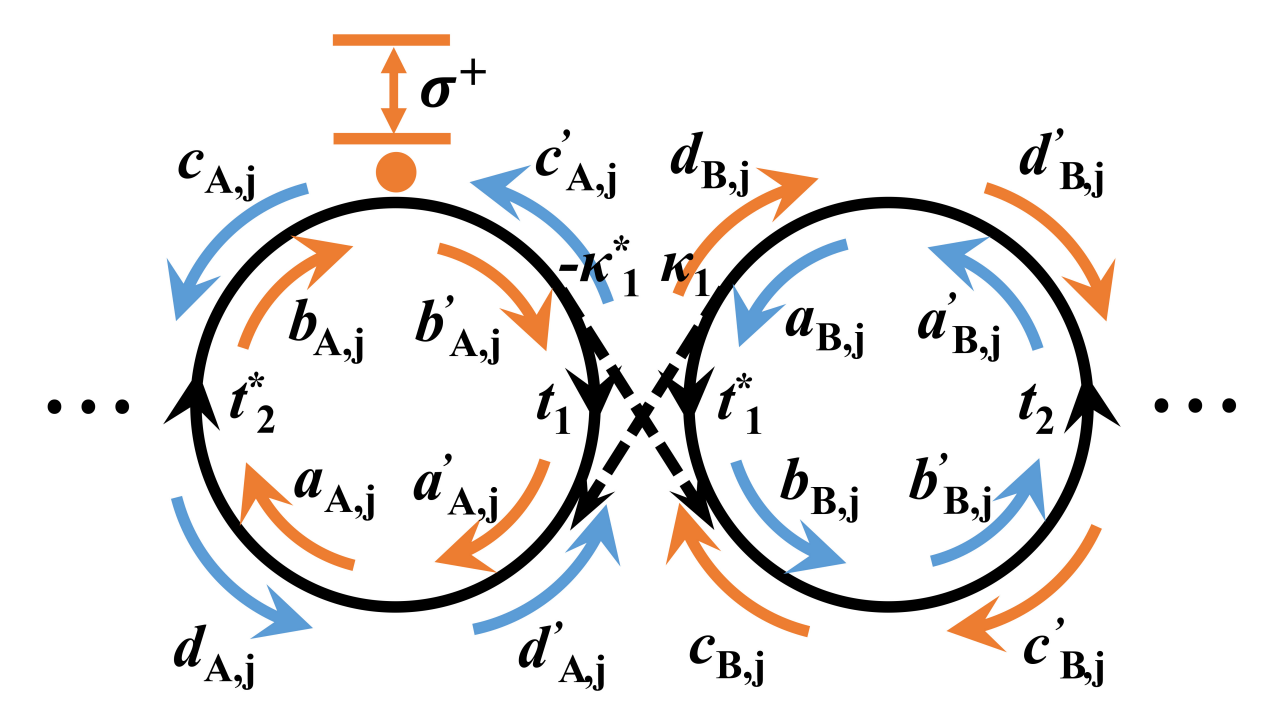


FIG. S1. The unit cell presented in the main text, with the sublattices A and B. The yellow/blue arrows represent the circulating direction of the clockwise/counterclockwise whispering-gallery modes.

Our chiral 1D-CROW system is shown in the main text. Each resonator, with a resonance frequency  $\Omega$  and an internal dissipation  $\gamma_{\rm in}$ , supports two degenerate optical whispering-gallery modes: clockwise and counterclockwise

modes. The adjacent resonators are separated by  $\Lambda$ . The resonators are divided into two groups A and B, where the A-sublattice resonator couples with a two-level QE in a chiral way and the B-sublattice resonator decouples from the QEs. As the light travels in the CROW, the excited propagation modes in the A and B sublattices are opposite, thus forming N unit cells. We assume that QEs couple to the clockwise mode in the A-sublattice resonator, but decouple from the counterclockwise mode.

The chiral QE-light interaction implies that only the clockwise-circulating single photon interacts with the QE and passes through it with a transmission coefficient  $t_{qe}$ ; but the counterclockwise-circulating single photon decouples from the QE. We can treat the QE in the resonator as a quantum scatterer in an optical waveguide [3]. Then, we obtain  $t_{qe}$  by calculating the single-photon transmission in the QE-waveguide system [4],

$$t_{\rm qe} = \frac{\omega - \omega_q + i(\gamma - \Gamma)}{\omega - \omega_q + i(\gamma + \Gamma)},\tag{S18}$$

where  $\omega$  ( $\omega_q$ ) is the central (resonance) frequency of the incident photon (the QE),  $\gamma$  is the dissipation rate of the QE.  $\Gamma$  is the decay rate from the QE into the resonator, and the QE-resonator coupling strength is  $g \approx \sqrt{2\Gamma \times \mathcal{F}}$  [3], where the  $\mathcal{F}$  is the free spectral range of the resonator.

Note that the chiral QE-light interaction leads to a vanishing reflection of the single-photon propagation [4]. The QEs can modify the phase and amplitude of the single-photon field propagating along the clockwise direction in the A-sublattice resonators, but do not excite the counterclockwise-circulating field via radiation as a normal achiral system.

Theoretically, the QE chirally coupled to the resonator can be treated as a "single-photon phase-amplitude modulator" [3]. For simplicity, we take  $t_{\rm qe} \equiv \exp(i\varphi)$  ( $\varphi = \varphi_1 + i\varphi_2$ ), where  $\varphi_1(\omega) = \arg(t_{\rm qe})$  and  $\exp(-\varphi_2) = |t_{\rm qe}|$  describe the changes in phase and amplitude, respectively. From Eq. (S18), we have  $|t_{\rm qe}| \approx 1$  and  $\varphi_2 \approx 0$  when  $\gamma \ll \Gamma$ . In this case, the QEs only change the phase  $\varphi_1$  of the single-photon field of the clockwise mode.

Then, using the notation from Fig. S1, we can write the transfer matrix formalism for the 1D-CROW system:

$$x_{j+1} = P_2 Q_2 P_1 Q_1 x_j. (S19)$$

Here,  $x_j = (a_{A,j} \ b_{A,j} \ c_{A,j} \ d_{A,j})^T$  is a vector of the wave-packet amplitudes. The above matrices  $\{P_1, P_2\}$  and  $\{Q_1, Q_2\}$  describe inter-sublattice and intra-sublattice transfer, respectively. We refer to  $P_{1,2}$  and  $Q_{1,2}$  as coupling and propagation matrices, and they can be written as:

$$P_1 = \begin{pmatrix} M_{c,1} & 0 \\ 0 & M_{c,1} \end{pmatrix}, \quad Q_1 = \begin{pmatrix} M_{p,A} & 0 \\ 0 & M_{p,B} \end{pmatrix},$$
 (S20a)

$$P_2 = \begin{pmatrix} M_{c,2} & 0 \\ 0 & M_{c,2} \end{pmatrix}, \quad Q_2 = \begin{pmatrix} M_{p,B} & 0 \\ 0 & M_{p,B} \end{pmatrix},$$
 (S20b)

$$M_{c,1} = \frac{1}{\kappa_1} \begin{pmatrix} 1 & -t_1 \\ t_1^* & -1 \end{pmatrix}, \quad M_{c,2} = \frac{1}{\kappa_2} \begin{pmatrix} 1 & -t_2 \\ t_2^* & -1 \end{pmatrix},$$
 (S20c)

$$M_{\mathrm{p,A}} = \begin{pmatrix} e^{-i\theta(R)} & 0\\ 0 & e^{i[\theta(R)+\varphi]} \end{pmatrix}, \quad M_{\mathrm{p,B}} = \begin{pmatrix} e^{-i\theta(R)} & 0\\ 0 & e^{i\theta(R)} \end{pmatrix}, \tag{S20d}$$

where  $\{t_1, t_2\}$  and  $\{\kappa_1, \kappa_2\}$  are the transmission and coupling coefficients of the intrasite and intersite resonators. According to waveguide mode coupling theory,  $t_{1/2}$  are real,  $\kappa_{1/2}$  are imaginary, and  $|t_{1/2}|^2 + |\kappa_{1/2}|^2 = 1$ . Note that the coupling strengths between resonators can be deduced from  $J_{1/2} = \text{Im}\left(\kappa_{1/2}\right) \times \mathcal{F}\left[3\right]$ . The factor  $\theta(L) = \pi \beta L$  is the propagation phase change dependent on the path L of the light propagating in the resonator, where  $\beta$  is the propagation constant, given by  $\beta = n_{\text{eff}}\omega/c$ . From Eqs. S20, we can find that the propagation modes in each resonator are decoupled. In other words, the transfer relation of the wave-packet amplitudes are only from (a,b) to  $\begin{pmatrix} a',b' \end{pmatrix}$  and from (c,d) to  $\begin{pmatrix} c',d' \end{pmatrix}$ . Therefore, when we consider one of them, we can study it in the form of a 2 × 2 matrix as shown in the main text.

Using Bloch's theorem [5, 6], we can obtain the eigenvalue equations of the system under two excitation modes (i.e., the  $CW_A - CCW_B$  supermode and the  $CCW_A - CW_B$  supermode),

$$Det|M_{c,2}M_{p,B}M_{c,1}M_{p,A} - \exp(-2iK\Lambda)| = 0,$$
(S21)

and

$$Det|M_{c,2}M_{p,B}M_{c,1}M_{p,B} - \exp(-2iK\Lambda)| = 0,$$
(S22)

respectively. Above, K is the Bloch quasi-momentum and  $2\Lambda$  is the unit spacing. Solving the above equations, we have the dispersion relation

$$\cos(2K\Lambda) = \left[\cos(2\theta) - t_1 t_2\right] / \kappa_1 \kappa_2 \tag{S23}$$

for the  $CCW_A - CW_B$  supermode and the dispersion relation

$$\cos\left(2K\Lambda - \frac{\varphi}{2}\right) = \left[\cos\left(2\theta + \frac{\varphi}{2}\right) - t_1 t_2 \cos\left(\frac{\varphi}{2}\right)\right] / \kappa_1 \kappa_2 \tag{S24}$$

for the  $CW_A - CCW_B$  supermode.

Obviously, the dispersion relation of the  $CW_A - CCW_B$  supermode is different from Eq. (S23). This nonreciprocal single-photon dispersion property occurs because the chiral QE-light coupling breaks the time-reversal symmetry of the system. In the  $CW_A - CCW_B$  supermode, the QE interacts with the single-photon evanescent field and introduces an additional propagating phase  $\varphi$  to the single-photon field. In contrast, this extra phase factor disappears in the  $CCW_A - CW_B$  supermode. In the absence of the QEs, we have  $\varphi = 0$  and then Eq. (S24) reduces to the reciprocal case Eq. (S23). In this case, the single-photon dispersion in two counter-propagating cases becomes reciprocal.

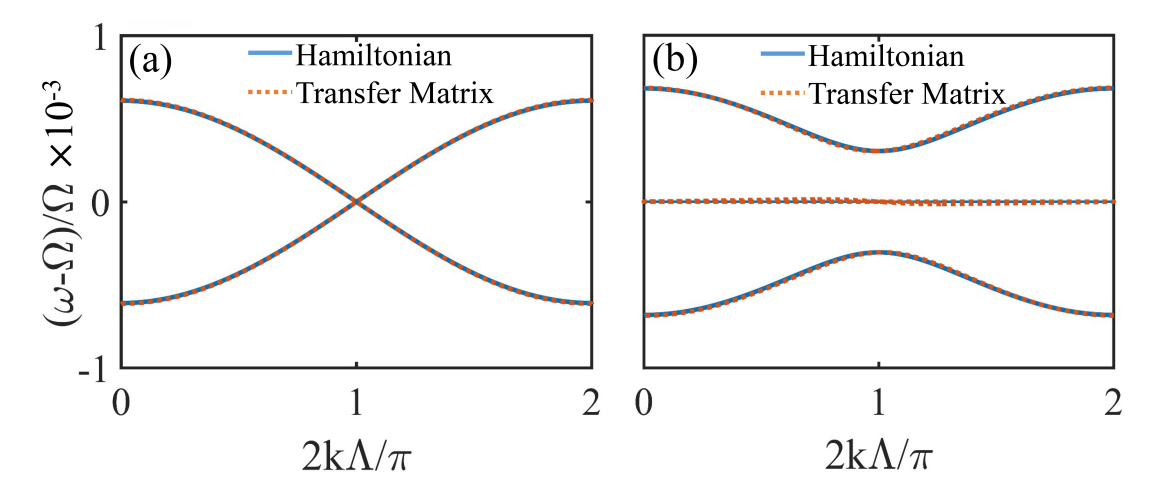


FIG. S2. The single-photon band structures calculated by the Hamiltonian and transfer matrix method, respectively. (a) The system is excited in the  $CCW_A - CW_B$  supermode and (b) is excited in the  $CW_A - CCW_B$  supermode. Other parameters are  $\Gamma/\Omega = 1.5 \times 10^{-5}$  corresponding to  $g/\Omega = 3 \times 10^{-4}$ ,  $\kappa_1 = \kappa_2 = 0.1i$  corresponding to  $J_1/\Omega = J_2/\Omega = 3 \times 10^{-4}$ , and  $\gamma = 0$ .

Now we consider a simple example,  $\kappa_1 = \kappa_2$ , which means that the coupling strengths between resonators are equal, i.e.,  $J_1 = J_2$ . Considering the resonators with a radius of r = 40 µm,  $\Omega/2\pi = 195$  THz and  $n_{\rm eff} = 2$ , we obtain  $\mathcal{F}/2\pi = 0.6$  THz. We take  $\kappa_1 = \kappa_2 = 0.1i$  and  $\Gamma/\Omega = 1.5 \times 10^{-5}$ , thus  $J_1/\Omega = J_2/\Omega = 3 \times 10^{-4}$  and  $g/\Omega = 3 \times 10^{-4}$ . These parameter settings are consistent with Fig. 4 in the main text. Figure S2 shows the single-photon band structures of our system under two different excitation modes. The red dotted curves are the dispersion relations corresponding to the real solutions of Eqs. (S23) and (S24). And the blue solid curves are the results of directly solving the eigenequations of the Hamiltonian. It can be found that the results of transfer matrix calculation are consistent with solving the eigenvalues and eigenstates of the Hamiltonian.

#### III. TUNNELING ENABLED SINGLE-PHOTON CIRCULATOR

In this section, we discuss the influence of edge-state tunneling. When a single photon enters port 1 or 3, it excites the  $CW_A - CCW_B$  supermode of the CROW, which corresponds to the forward input, see Fig. 1 in the main text. The photon incident to ports 2 and 4 (backward input) excites the oppositely propagating mode, i.e., the  $CCW_A - CW_B$  supermode. We consider the case with edge states, that is  $J_1 < J_2$ . As the discussion in the main text, the edge states in our chiral QE-CROW system exhibit a nonreciprocal characteristic. This unique property can be used to achieve a single-photon circulator via single-photon edge-state tunneling effect.

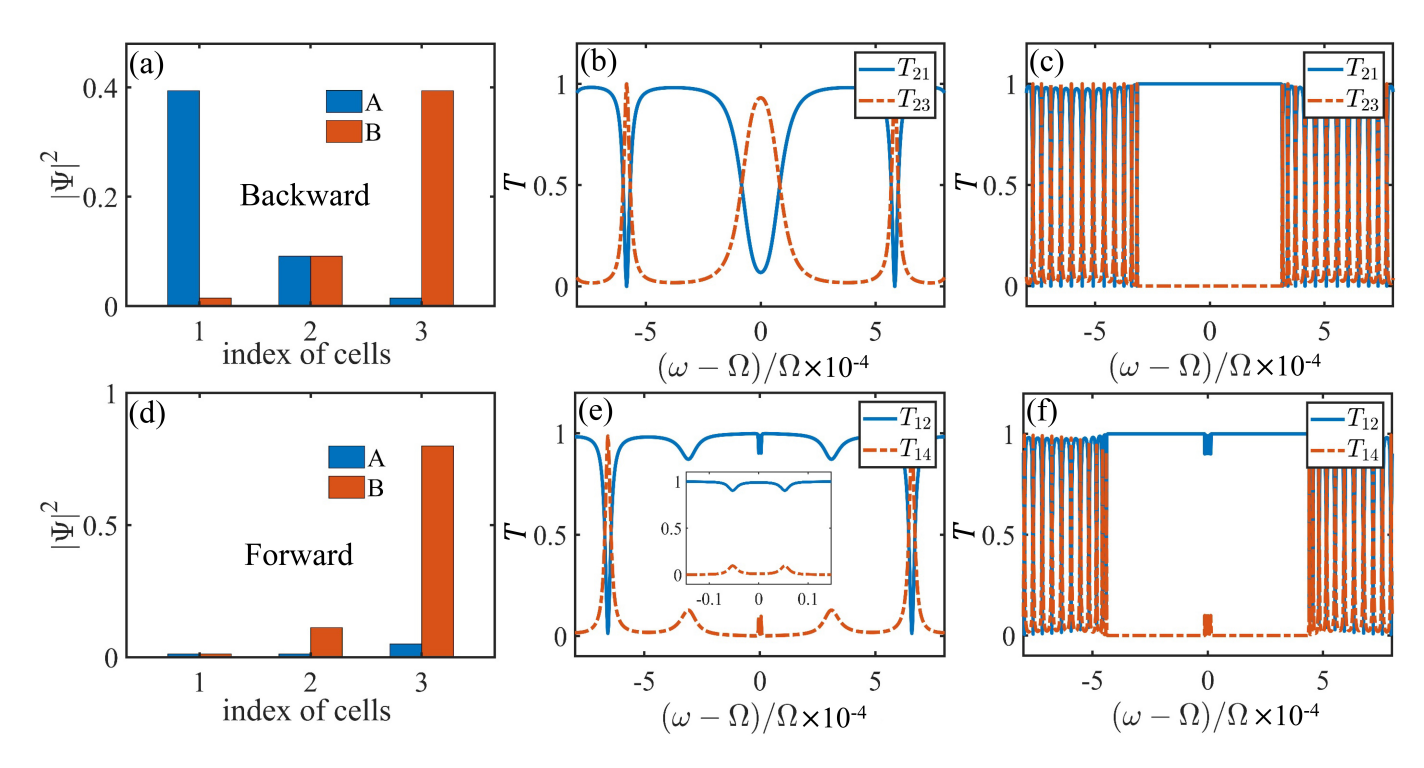


FIG. S3. Nonreciprocal probability distribution and transmission of the chiral QE-CROW system at zero-energy frequency. (a-c) for the backward input without coupling to the QEs, g = 0. (d-f) for the forward input with coupling to the QEs,  $g/\Omega = 3 \times 10^{-4}$ . The number of cells is N = 3 in (a, b, d, e) and N = 20 in (c, f). Other parameters are  $J_1/\Omega = 3 \times 10^{-4}$ ,  $J_2 = 2J_1$ .

In the backward case, the QEs have no interaction with the resonators. The two degenerate zero-energy eigenstates are odd and even superpositions of states localized exponentially on the left and right boundaries. When the number of cells is small, such as N=3, there is an exponentially small overlap between the left and right edges [7], see Fig. S3(a). This leads to a probability that the photon passes through the CROW, that is, an edge-state tunneling. In stark contrast, there is negligible overlap of left and right edge states at the zero-energy frequency, as shown in Fig. S3(d), because of the energy splitting of left edge state. Due to the coupling with the QEs, the left single-photon edge state becomes a doublet with an energy splitting proportional to the coupling strength g, while the energy of the right single-photon edge state is still zero. Therefore, this edge-state tunneling effect disappears at the zero-energy frequency in the forward case.

Figures S3(b) and (e) show the nonreciprocal single-photon transmission at the zero-energy frequency induced by edge-state tunneling in the number of cells N=3. When a single photon is incident to port 2, corresponding to the backward case, the transmission  $T_{23}$  can reach about 0.93 because of the edge-state tunneling effect, see Fig. S3(b). But for the forward input, i.e., the single photon entering port 1, the light cannot enter the CROW at all, and thus  $T_{14} \approx 0$  ( $T_{12} \approx 1$ ), see Fig. S3(e). Due to the symmetry of the CROW, we have  $T_{34} = T_{12}$  and  $T_{41} = T_{23}$ . As a result, we can construct a single-photon circulator using the edge-state tunneling with a circling photon transport  $1 \rightarrow 2 \rightarrow 3 \rightarrow 4 \rightarrow 1$  at the zero-energy frequency. The fidelity and the average photon survival probability of the circulator are calculated as  $\{0.96, 0.99\}$ . The negligible transmission near the zero energy in the inset of Fig. S3(e) results from the single-photon flat band. The small dips appearing at  $(\omega - \Omega) = \pm g$  correspond to the eigenvalue of the left edge states, and their depth decreases with increasing QE-resonator coupling strength g.

When the number of cells becomes large, this edge-state tunneling vanishes for the backward case due to the absence of overlap between the left and right edges. In this case, the single-photon circulator cannot be constructed at zero-energy frequency, see Figs. S3(c) and (f). The slight transmission at zero energy in Fig. S3(f) is caused by the single-photon flat band for the forward input.

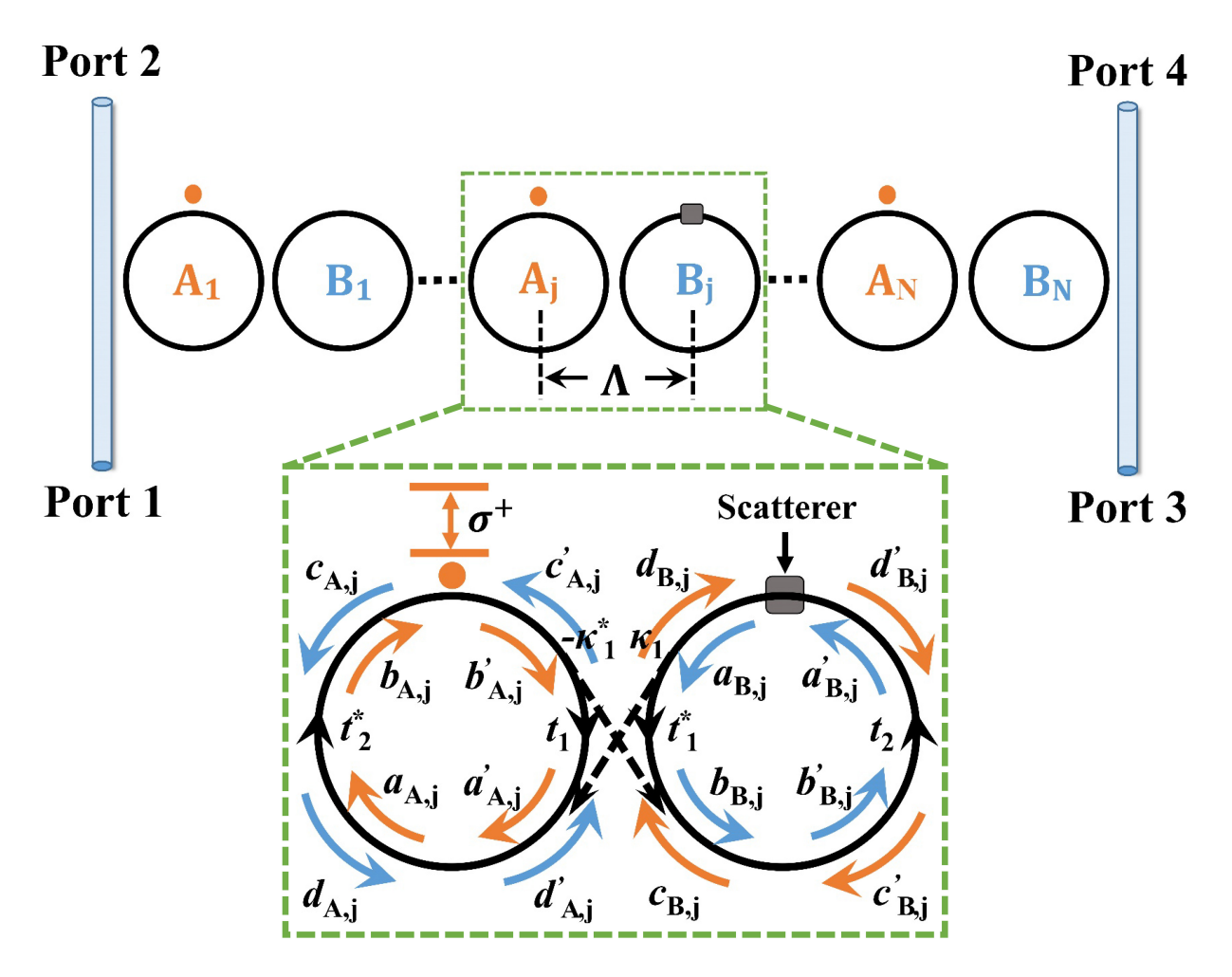


FIG. S4. Schematic of a chiral QE-CROW system containing N unit cells and the input and output waveguides. Inset: we position one scatterer in the middle of the B-sublattice resonator.

### IV. THE EFFECT OF THE SCATTERER

In this section, we discuss the effect of the scatterer in our chiral 1D-CROW system shown in Fig. S4. We position one scatterer in the B-sublattice resonator in the middle cell of the CROW. The scatterer will couple the two fields of CW and CCW modes in the B-sublattice resonator. Therefore, the transfer matrix of the scatterer which couples the (a, b) and (c, d) fields together is given by

$$Q_{\text{scatt}} = \frac{1}{t_s} \begin{pmatrix} 1 & 0 & 0 & -r_s \\ 0 & 1 & 0 & 0 \\ 0 & 0 & 1 & 0 \\ r_s & 0 & 0 & 1 \end{pmatrix} , \tag{S25}$$

where  $t_s$  and  $r_s$  are the transmission and reflection coefficients introduced by the scatterer, respectively. They satisfy  $|t_s|^2 + |r_s|^2 = 1$  when the dissipation of the scatterer is neglected [3, 6]. We assume the scatterer to be weak, thus we have

$$t_s = \cos \epsilon \approx 1 - \frac{\epsilon^2}{2}, \quad r_s = i \sin \epsilon \approx i\epsilon,$$
 (S26)

with  $\epsilon \ll 1$ . The coupling strength of the backscattering can be derived as  $h = \epsilon \times \mathcal{F}$  [3].

The input and output coupling matrices between the resonators and the waveguides,  $P_{\rm in}$  and  $P_{\rm out}$ , can be written

as

$$P_{\rm in} = \frac{1}{\kappa_{\rm in}} \begin{pmatrix} -t_{\rm in} & 1 & 0 & 0\\ -1 & t_{\rm in}^* & 0 & 0\\ 0 & 0 & -t_{\rm in} & 1\\ 0 & 0 & -1 & t_{\rm in}^* \end{pmatrix}, \quad P_{\rm out} = \frac{1}{\kappa_{\rm out}} \begin{pmatrix} 1 & -t_{\rm out} & 0 & 0\\ t_{\rm out}^* & -1 & 0 & 0\\ 0 & 0 & 1 & -t_{\rm out}\\ 0 & 0 & t_{\rm out}^* & -1 \end{pmatrix},$$
(S27)

where  $\{t_{\rm in}, t_{\rm out}, \kappa_{\rm in}, \kappa_{\rm out}\}$  are the transmission and coupling coefficients and they satisfy  $|t_{\rm in/out}|^2 + |\kappa_{\rm in/out}|^2 = 1$ . Without loss of generality, we put the scatterer in the middle of the B-sublattice resonator, see the inset in Fig. S4. Therefore, the transfer matrix of the unit cell is given by:

$$C_{\text{middle}} = P_2 \cdot Q_2 \left(\frac{R}{2}\right) \cdot Q_{\text{scatt}} \cdot Q_2 \left(\frac{R}{2}\right) \cdot P_1 \cdot Q_1 \left(R\right) . \tag{S28}$$

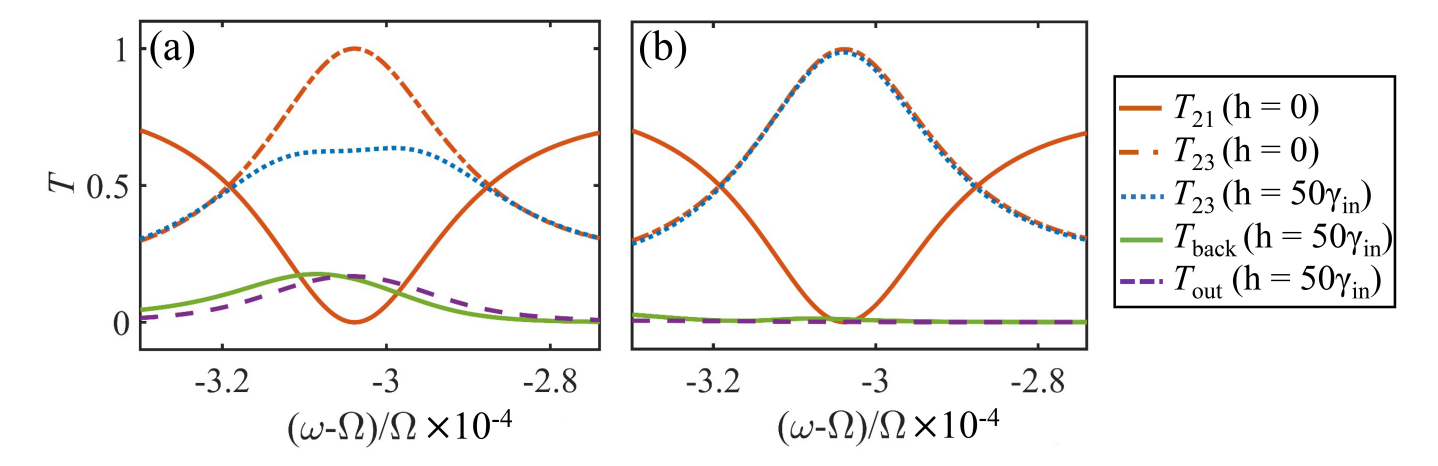


FIG. S5. Robust one-way transmission of the chiral QE-CROW system. Single-photon transmission in the conventional 1D CROW without coupling the QEs (a) and in a chiral QE-CROW system (b). Other parameters are N=10,  $\Gamma/\Omega=1.5\times10^{-5}$   $(g/\Omega=3\times10^{-4})$ ,  $\kappa_1=\kappa_2=0.1i$   $(J_1/\Omega=J_2/\Omega=3\times10^{-4})$ ,  $\kappa_{\rm in}=\kappa_{\rm out}=0.25i$ , and  $\gamma=0$ .

We consider a scatterer embedded in the middle cell of a chiral QE-CROW system, with  $N=10,\ r=40$  µm,  $\Omega/2\pi=195$  THz, and  $n_{\rm eff}=2$ . The free spectral range of the resonator is calculated as  $\mathcal{F}/2\pi=0.6$  THz. We take  $\Gamma/\Omega=1.5\times 10^{-5},\ \kappa_1=\kappa_2=0.1i,$  and  $\kappa_{\rm in}=\kappa_{\rm out}=0.25i,$  so  $g/\Omega=3\times 10^{-4},\ J_1/\Omega=J_2/\Omega=3\times 10^{-4}$  and the external dissipations of resonators can be calculated as  $\gamma_{\rm ex}/2\pi=19.4$  GHz [setting  $\gamma_{\rm in}=0.02\gamma_{\rm ex},$  thus  $\gamma_{\rm tol}/2\pi=(\gamma_{\rm ex}+\gamma_{\rm in})/2\pi=19.8$  GHz [3]. These parameter settings are consistent with Fig. 4 in the main text.

The single-photon transmission in our system is robust against backscattering. To justify this, we compare the transmission  $T_{23}$  and the backscattering of our chiral QE-CROW system and a conventional CROW system. This scatterer induces a strong backscattering  $h=50\gamma_{\rm in}$  between the CW and CCW mode in the resonator. The single photon inputs to port 2. In the conventional CROW system equivalent to the case without the QEs, see Fig. S5(a), the scatterer causes a considerable decrease in the transmission  $T_{23}$ , reducing it from unity to 0.63. The backscattering also generates a reflection to port 2 and unwanted photon transport to port 4 with equal probability about 18%. In stark contrast, as shown in Fig. S5(b), the scatterer has little influence on photon transmission in our system because the chiral QE-light interaction results in a large frequency splitting  $\Delta\Omega$  in the A-sublattice resonator.

#### V. INFLUENCE OF THE NUMBER OF UNIT CELLS

In this section, we study the effect of the number of unit cells N on the frequency-multiplexing channels of the single-photon circulator.

On the one hand, as we discussed in the main text, when the single photon is incident into port 2, the excited  $CCW_A - CW_B$  modes decouple from the QEs. In this case, the number of transmitted peaks and dips formed is proportional to 2N, see Figs. S6(a) and (c) for N = 5 and N = 20, respectively.

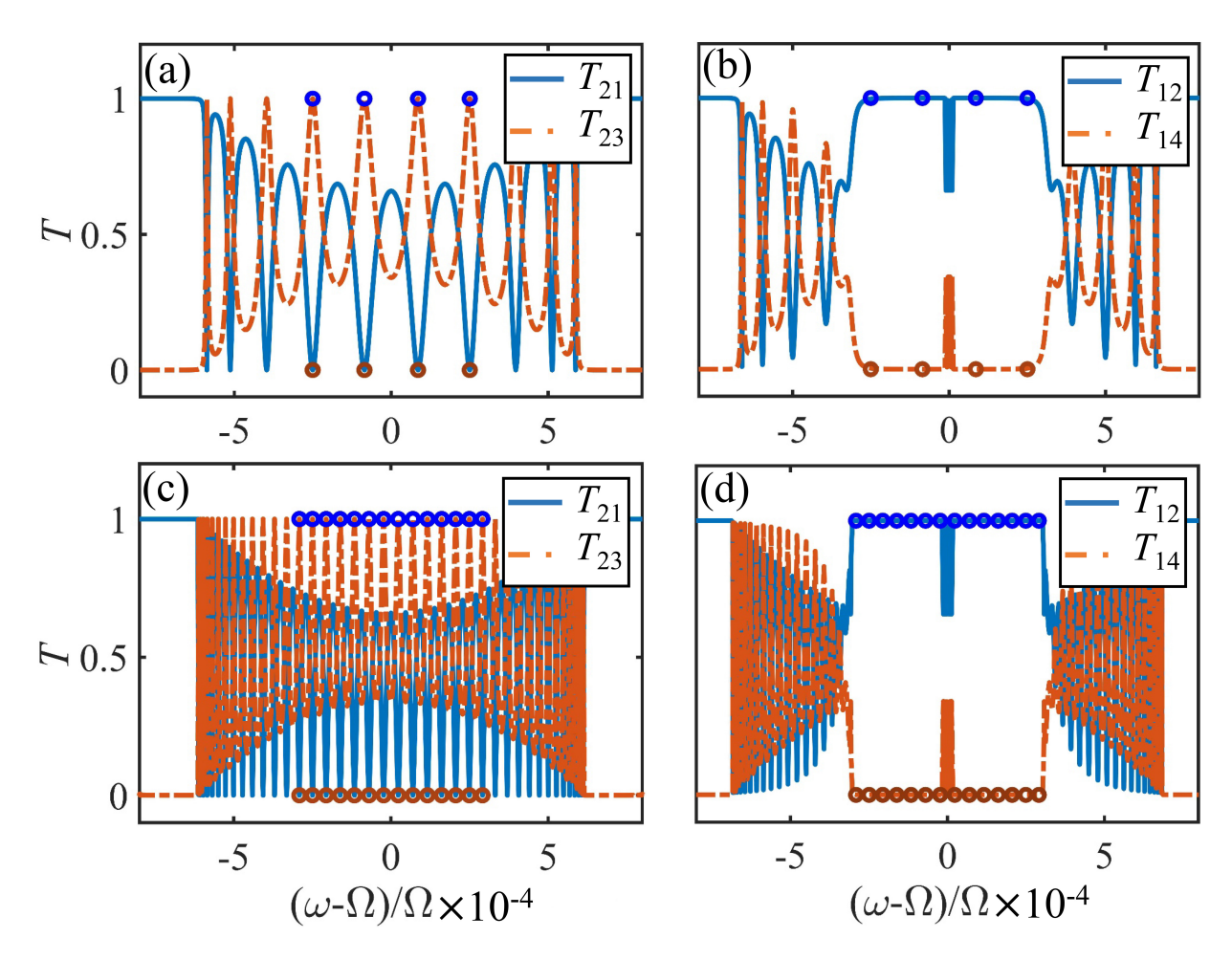


FIG. S6. Transmission of the chiral QE-CROW system with N=5 in (a) and (b) and N=20 in (c) and (d). In (a) and (c) the single photon incidents to port 2. In (b) and (d) the single photon incidents port 1 with  $\Gamma/\Omega=1.5\times10^{-5}$ . Other parameter are  $\gamma=0$ ,  $\kappa_{\rm in}=\kappa_{\rm out}=0.25i$ , and  $\kappa_1=\kappa_2=0.1i$ .

On the other hand, the bandwidth of the edge state formed by the input in the opposite direction, i.e., port 1, depends only on the QE-resonator coupling strength g, and does not depend on the number of unit cells. Therefore, at a given decay rate  $\Gamma$  for determining the QE-resonator coupling strength by  $g \approx \sqrt{2\Gamma \times \mathcal{F}}$ , we can increase and adjust the frequency-multiplexing channels of the single-photon circulator by increasing the number of cells N. For example, there are 4 and 14 nonreciprocal windows for N=5 and N=20 with  $\Gamma/\Omega=1.5\times 10^{-5}$ , see the blue dots in Figs. S6(b) and (c), respectively.

<sup>[1]</sup> Y. Peng, Y. Bao, and F. von Oppen, Boundary Green functions of topological insulators and superconductors, Phys. Rev. B **95**, 235143 (2017).

<sup>[2]</sup> V. M. Martinez Alvarez and M. D. Coutinho-Filho, Edge states in trimer lattices, Phys. Rev. A 99, 013833 (2019).

<sup>[3]</sup> J. Tang, L. Tang, and K. Xia, Single-photon transport in a whispering-gallery mode microresonator directionally coupled with a two-level quantum emitter, arXiv preprint arXiv:2110.09375 (2021).

<sup>[4]</sup> K. Xia, G. Lu, G. Lin, Y. Cheng, Y. Niu, S. Gong, and J. Twamley, Reversible nonmagnetic single-photon isolation using unbalanced quantum coupling, Phys. Rev. A 90, 043802 (2014).

<sup>[5]</sup> J. K. S. Poon, J. Scheuer, S. Mookherjea, G. T. Paloczi, Y. Huang, and A. Yariv, Matrix analysis of microring coupled-resonator optical waveguides, Opt. Express 12, 90 (2004).

<sup>[6]</sup> M. Hafezi, E. A. Demler, M. D. Lukin, and J. M. Taylor, Robust optical delay lines with topological protection, Nat. Phys. 7, 907 (2011).

<sup>[7]</sup> J. K. Asbóth, L. Oroszlány, and A. Pályi, A short course on topological insulators, Lecture notes in physics 919, 166 (2016).